

Exploring Oxidation in the Remote Free Troposphere: Insights From Atmospheric Tomography (ATom)

W. H. Brune¹, D. O. Miller¹, A. B. Thames¹, H. M. Allen², E. C. Apel³, D. R. Blake⁴, T. P. Bui⁵, R. Commane⁶, J. D. Crouse², B. C. Daube⁷, G. S. Diskin⁸, J. P. DiGangi⁸, J. W. Elkins⁹, S. R. Hall³, T. F. Hanisco¹⁰, R. A. Hannun^{11;10}, E. J. Hintsa^{12;9}, R. S. Hornbrook³, M. J. Kim¹³, K. McKain^{12;9}, F. L. Moore^{12;9}, A. Neuman^{14,12}, J. M. Nicely^{15;10}, J. Peischl^{12;14}, T. B., Ryerson¹⁴, J. M. St. Clair^{11,10}, C. Sweeney⁹, A. P. Teng^{13,16}, C. Thompson^{17;12;14}, K. Ullmann³, P. R. Veres¹⁴, P. O. Wennberg¹³, and G. M. Wolfe^{11;10}

¹Department of Meteorology and Atmospheric Science, Pennsylvania State University, University Park, PA, USA

²Division of Chemistry and Chemical Engineering, California Institute of Technology, Pasadena, CA, USA

³Atmospheric Chemistry Observations and Modeling Laboratory, National Center for Atmospheric Research, Boulder, CO, USA

⁴Department of Chemistry, University of California, Irvine, CA, USA

⁵Earth Science Division, NASA Ames Research Center, Moffett Field, CA, USA

⁶Department of Earth and Environmental Sciences of Lamont-Doherty Earth Observatory, Columbia University, Palisades, NY, USA

⁷Department of Earth and Planetary Sciences, Harvard University, Cambridge, MA, USA

⁸Chemistry and Dynamics Branch, NASA Langley Research Center, Hampton, VA, USA

⁹Global Monitoring Division, Earth System Research Laboratory, NOAA, Boulder, CO, USA

¹⁰Atmospheric Chemistry and Dynamics Laboratory, NASA Goddard Space Flight Center, Greenbelt, MD, USA

¹¹Joint Center for Earth Systems Technology, University of Maryland, Baltimore County, Baltimore, MD, USA

¹²Cooperative Institute for Research in Environmental Sciences, University of Colorado Boulder, Boulder, CO, USA

¹³Division of Geological and Planetary Sciences, California Institute of Technology, Pasadena, CA, USA

¹⁴Chemical Sciences Division, Earth System Research Laboratory, NOAA, Boulder, CO, USA,

¹⁵Earth System Science Interdisciplinary Center, University of Maryland, College Park, MD, USA

¹⁶Now with Divergent 3D, Los Angeles, CA, USA

¹⁷Now with Scientific Aviation, Boulder, CO, US

Contents of this file

Figures S1 to S9

Tables S1 to S2

Detailed description of the OH Scavenging Inlet (OHSI), including Figure S10

Introduction

This supporting information consists of figures, tables, and a technical description of the OH Scavenging Inlet that provide more detail than is in the paper itself. They are not essential for understanding the descriptions or analysis in the paper, but provide interested readers more detail or illustrations supporting the text in the paper. These figures and tables were produced using the same data and software that were used to produce the figures and tables in the paper itself.

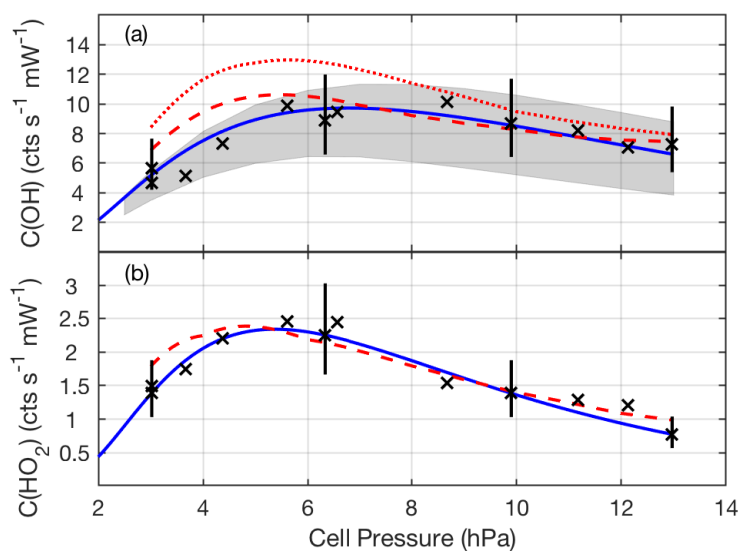


Figure S1. Laboratory-based calibration curves for (a) OH and (b) HO₂ as a function of detection cell pressure, which is roughly proportional to atmospheric pressure. Different detection cell pressures are generated by changing the inlet sizes, as described in detail in Faloon et al. (2004). Blue lines are the fits of the calibration measurements for the OH and HO₂ signals produced by the mixing ratios. The x symbols are calibration data and the vertical bars are the uncertainty at 2σ confidence. The grey shading is the range of OH calibrations from five previous NASA DC-8 aircraft missions. The red dashed lines are the calibration curves that would be needed to force agreement between the median observed and modeled OH and HO₂ for all ATom phases at all altitudes. For ATom-1, the OH calibration to force agreement would need to be 20% higher than that for the median (red dotted curve), well above any previous calibrations at cell pressures below 7 hPa.

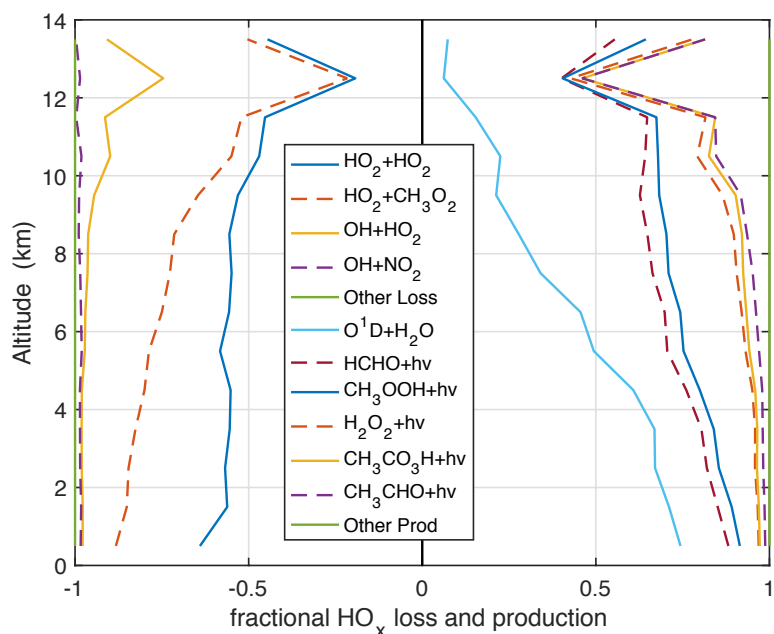


Figure S2. Fractional HO_x loss and production for ATom-1. The fractional loss or production for each term is the difference between it and the line for the preceding term closer to zero. The first five terms are loss, the second seven terms are production. Smaller production and loss term have been added together to form “Other Loss” and “Other Prod”.

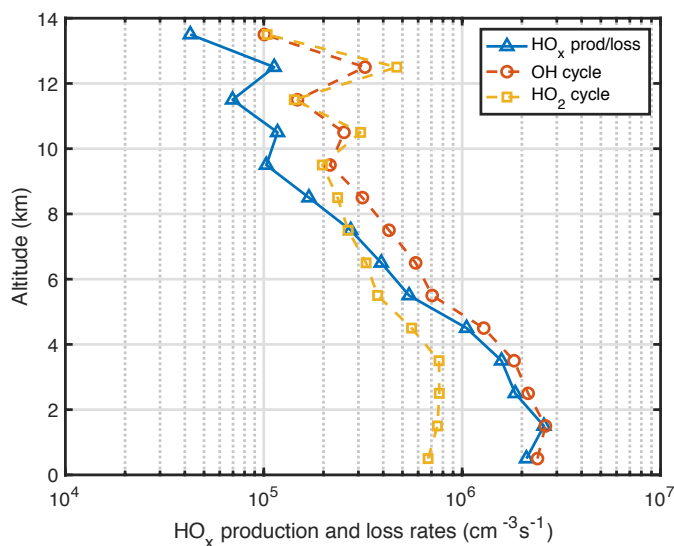


Figure S3. Median modeled HO_x production, which equals modeled HO_x loss (triangles), OH cycling to HO_2 (circles), and HO_2 cycling to OH (squares) as a function of altitude for ATom 1. Figures for ATom 2, 3, and 4 are similar. HO_x cycling is faster than HO_x production above 8 km where median NO abundances were higher, but not below 8 km where NO abundances were lower. Below 4 km, HO_x production is mainly by OH production, OH reactions then shift HO_x to HO_2 , and HO_x loss is mainly by HO_2 loss, with little HO_x recycling.

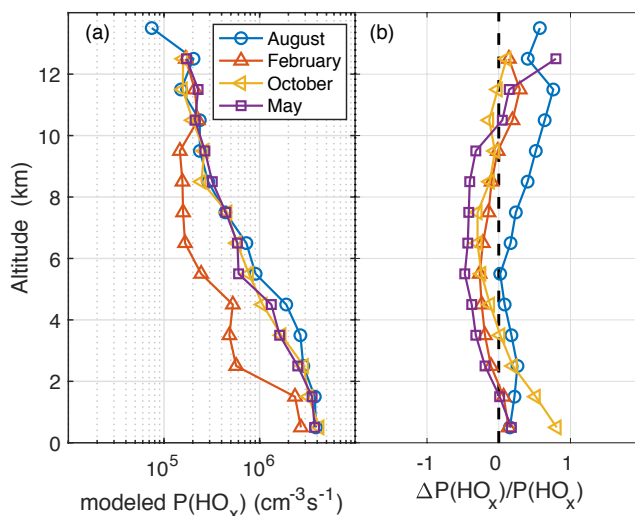


Figure S4. Median midday altitude profiles of (a) the modeled HO_x production rates and (b) the fractional changes in the modeled HO_x production rates necessary to achieve agreement between observed and modeled HO_x.

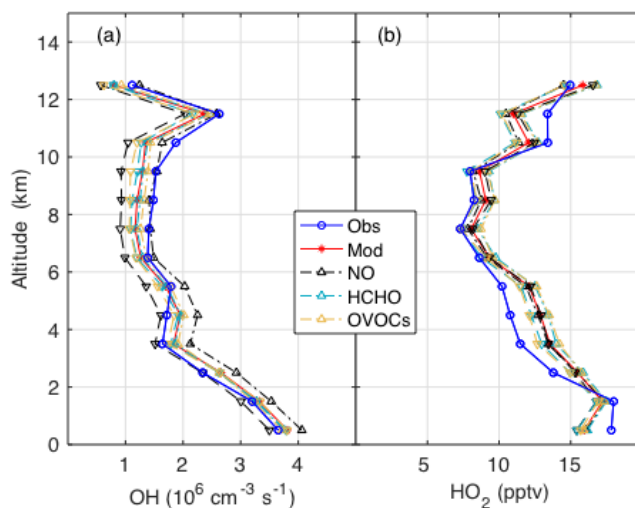


Figure S5. Sensitivity of (a) OH and (b) HO₂ as a function of altitude to the uncertainty in NO (black), HCHO by NASA ISAF (aqua), and OVOCs by TOGA and CIT-CIMS (gold) for ATom-2. Median values are found over each 0.5 km band for modeled (red stars) and observed (blue circles) OH and HO₂. The model sensitivity was tested by running the model with NO, TOGA OVOCs, and CIT-CIMS OVOCs at their stated 2 σ uncertainty limits. Upright triangles indicate measured value plus the 2 σ uncertainty and inverted triangles indicate measured value minus the 2 σ uncertainty.

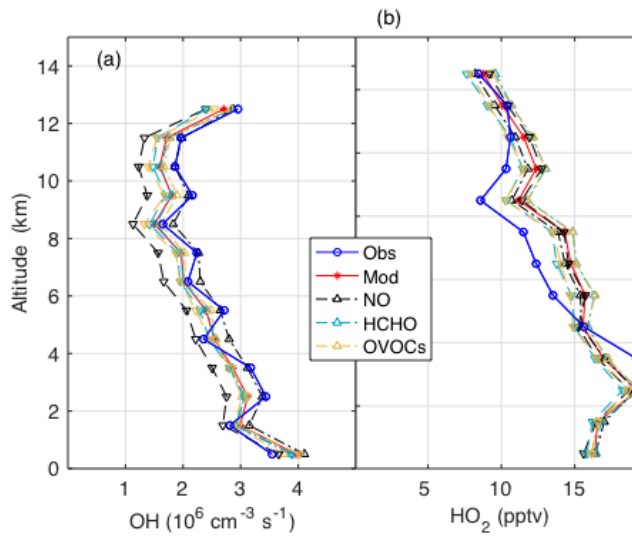


Figure S6. Sensitivity of (a) OH and (b) HO₂ as a function of altitude to the uncertainty in NO (black), HCHO by NASA ISAF (aqua), and OVOCs by TOGA and CIT-CIMS (gold) for ATom-3, as in Figure S5.

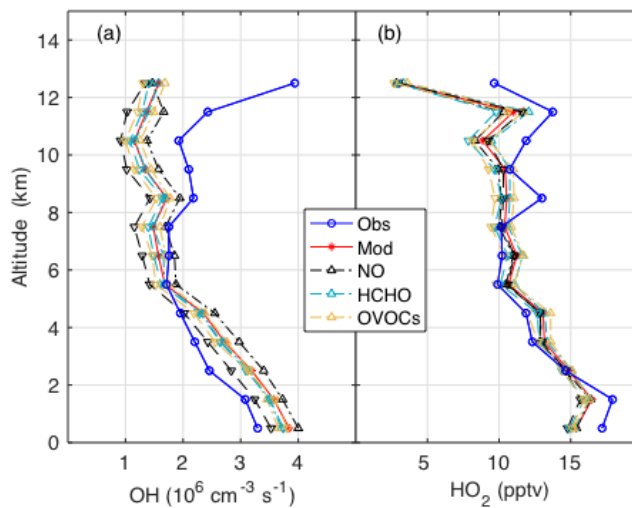


Figure S7. Sensitivity of (a) OH and (b) HO₂ as a function of altitude to the uncertainty in NO (black), HCHO by NASA ISAF (aqua), and OVOCs by TOGA and CIT-CIMS (gold) for ATom-4, as in Figure S5.

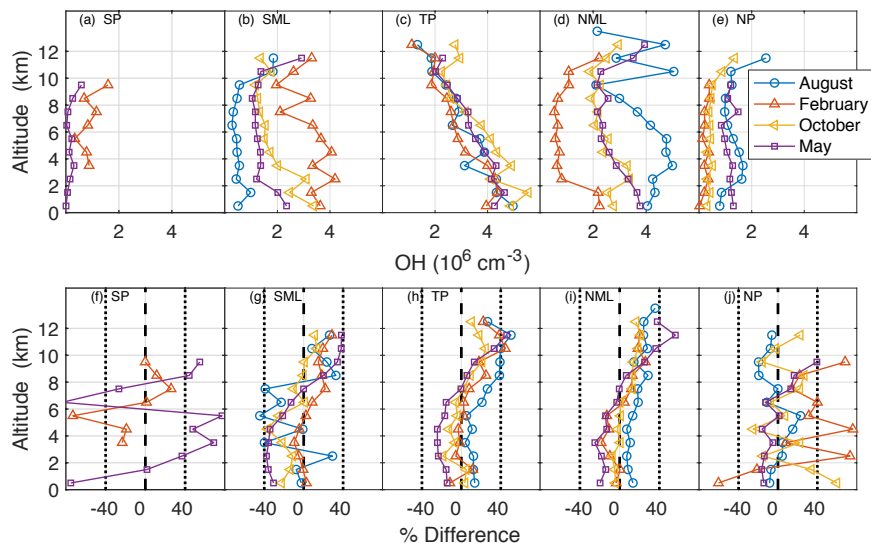


Figure S8. Median midday altitude profiles of OH (a-e) and the percent difference (Eq. 1) between observed and modeled OH (f-j) in 5 latitude bins for the 4 ATom periods using TOGA HCHO measurements instead of ISAF measurements (Table 1). Vertical dotted lines (f-j) indicate uncertainty (2σ confidence) in the percent difference due to model and measurement uncertainty.

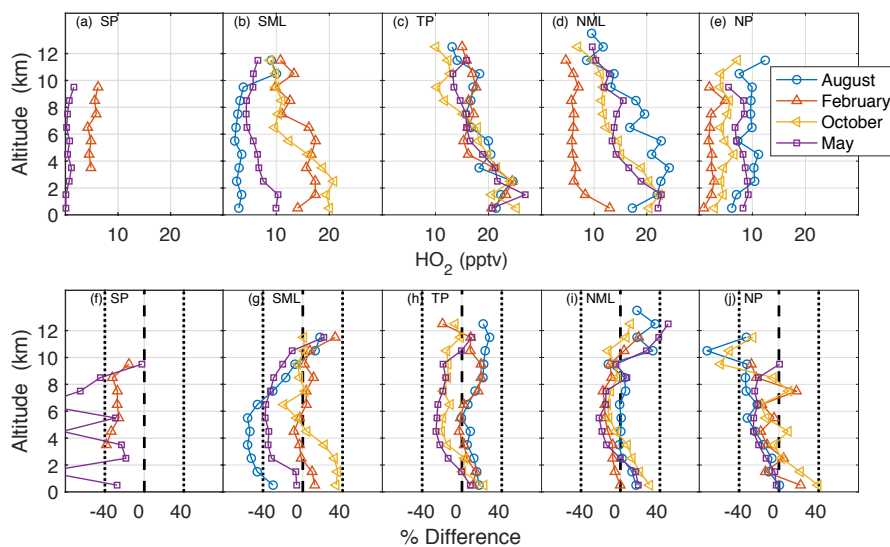


Figure S9. Median midday altitude profiles of HO₂ (a-e) and the percent difference (Eq. 1) between observed and modeled HO₂ (f-j) in 5 latitude bins for the 4 ATom periods using TOGA HCHO measurements instead of ISAF measurements (Table 1). Vertical dotted lines (f-j) indicate uncertainty (2σ confidence) in the percent difference due to model and measurement uncertainty.

Table S1. Details of airborne missions that included OH and/or HO₂ measurements

Study (Acronym) (reference for HO _x results)	When	Where	Why
Aerosol Characterization Experiment (ACE-1) (Mauldin et al., 1998)	October-December 1995	Tasmania, Australia and nearby ocean	Aerosol chemical, physical, and radiative properties
Stratospheric Traces of Atmospheric Transport (STRAT) (Wennberg et al., 1998; Jaeglé et al., 2001)	October 1995 – February 1996	Northern Pacific – Hawaii and California	Long-lived tracers in the lower stratosphere / upper troposphere
Subsonic Aircraft: Contrail and Cloud Effects Special Study (SUCCESS) (Brune et al., 1998; Jaeglé et al., 1998)	April – May 1996	Central United States	Cirrus clouds and contrails, aircraft exhaust composition
Pacific Exploratory Mission Tropics-A (PEM Tropics-A) (Mauldin et al., 1999; Chen et al., 2001)	August – October 1996	Remote Pacific	Remote troposphere composition
Subsonic Assessment Ozone and Nitrogen Oxide Experiment (SONEX) (Jaeglé et al., 2000; Faloon et al., 2000)	October – November 1997	North Atlantic flight corridor	Aircraft impact on tropospheric chemistry
Pacific Exploratory Mission Tropics-A (PEM Tropics-B) (Davis et al., 2001; Tan et al., 2001)	March – April, 1999	Remote Pacific	Remote troposphere composition
Tropospheric Ozone Production about the Spring Equinox (TOPSE) (Cantrell et al., 2003a; Cantrell et al., 2003b)	February – May 2000	North America to Arctic	Photochemistry of the springtime arctic troposphere
Transport and Chemical Evolution over the Pacific (TRACE-P) (Cantrell et al., 2003c; Olson et al., 2004)	February – April, 2001	Southeast Asia	Tropospheric chemistry near pollution source

Intercontinental Chemical Transport Experiment - North America (INTEX-A) (Ren et al., 2008)	July-August, 2004	Eastern United States	Tropospheric chemistry near pollution source
Intercontinental Chemical Transport Experiment - B (INTEX-B) (Adhikary et al., 2010)	March – May, 2006	(1) Northern Pacific; (2) Gulf of Mexico	(1) Transport of Asian pollution to North America; (2) Pollution in southern US and Mexico
African Monsoon Multidisciplinary Analysis (AMMA) (Stone et al., 2010)	July – August, 2006	West Africa	HO _x chemistry in relatively low NO _x and high biogenic VOC environment
HO _x Over Europe -2 (HOOVER 2) (Regelin et al., 2013)	July 2007	Central Europe	Photochemistry in the upper troposphere over Europe
Arctic Research of the Composition of the Troposphere from Aircraft and Satellites (ARCTAS) (Olson et al., 2012; Ren et al., 2012)	April – June, 2008	(1) Arctic (2) Western Canada	(1) Arctic pollution (2) Effects of wild fires and other emission sources
Oxidant and Particle Photochemical Processes (OP3) (Stone et al., 2011)	July, 2008	Over and around Borneo	Atmospheric oxidation in low NO _x and high isoprene environments
ROle of Nighttime chemistry in controlling the Oxidising Capacity of the AtmOsphere (RONOCO) (Stone et al., 2014b).	July 2010; January 2011	Over and downwind of the UK	Nighttime chemistry involving OH, HO ₂ , NO ₃ , and N ₂ O ₅
Deep Convective Clouds and Chemistry (DC3) (Brune et al., 2018)	May – June, 2012	Central United States	Impact of deep convective clouds on chemistry
KORUS-AQ	May-June 2016	Over and around South Korea	Asian pollution affecting South Korea
Atmospheric Tomography (ATom-1; -2; -3; -4)	August, 2016 – April, 2018	Pole-to-pole, down the Pacific, up the Atlantic	Typical global tropospheric chemistry

Table S2. Simultaneous measurements used to constrain the box model

Measurement	Instrument	Uncertainty (2σ confidence)	Reference
T p	MMS	± 0.5 C ± 0.3 hPa	Chan et al., 1998
H ₂ O	DLH (laser absorption)	$\pm 15\%$	Diskin et al., 2003
photolysis frequencies (30 measurements)	CAFS (Spectrometer)	$\pm (12-25)\%$, species dependent; (jNO ₂ : $\pm 12\%$); (jO(¹ D): $\pm 25\%$) (jH ₂ O ₂ : $\pm 15\%$) (jHCHO: $\pm 15\%$)	Shetter and Mueller, 1999
NO	NO _y O ₃ (Chemiluminescence)	6.6 pptv	Ryerson et al., 2000
O ₃	NO _y O ₃ [#] (UV absorption) UCATS (UV absorption)	1.4 ppbv $\pm 1-5\% + 1.5-2$ ppbv	Ryerson et al., 2000
CO	QCLS [#] (Laser absorption) NOAA Picarro (Spectrometer) UCATS (GC)	3.5 ppbv 3.6 ppbv 3.8 ppbv	Santorini et al., 2014 H. Chen et al., 2013
H ₂ O ₂ [*] , CH ₃ OOH [*] , CH ₃ CO ₃ H [*] , HNO ₃ SO ₂	CIT CIMS (CIMS)	$\pm 30\% + 50$ pptv 244.0 pptv	Crouse et al., 2006
HCOOH BrO	NOAA CIMS (CIMS)	$\pm 15\% + 50$ pptv $\pm 25\% + 0.2$ pptv	Neuman et al., 2016
CH ₄	NOAA Picarro [#] (Spectrometer) UCATS (GC) PANTHER (GC)	0.7 ppbv 12.4 ppbv 16.6 ppbv	H. Chen et al., 2013
HCHO	NASA ISAF [#] (LIF)	$\pm 10\% \pm 10$ pptv	Cazorla et al., 2015
methyl nitrate, ethyl nitrate, isoprene, acetylene, ethylene, ethane, propane, i-butane, n-butane, i-pentane, n-pentane, n-hexane, n-heptane, benzene, toluene, methyl chloride, methylene chloride, chloroform, methyl bromide, methyl chloroform,	UCI WAS (Whole air sampling; laboratory GC analysis)	$\pm 10\%$ (methyl nitrate & chloroform: $\pm 20\%$)	Colman et al., 2001

perchloroethene, 1,2-dichloroethane, DMS			
methanol*, formaldehyde, acetaldehyde*, ethyl benzene, toluene, methacrolein, methyl ethyl ketone, methyl tert-butyl ether, ethanol*, acetone*, 2-methylpentane, 3-methylpentane, 2,2,4-trimethylpentane, isobutene+1-butene, m-xylene+p-xylene, o-xylene, tricyclene, limonene+D3-carene, propanal*, butanal*, acrolein*	TOGA (GC, Spectrometer)	± 15-50% (acetaldehyde: ± 20%)	Apel et al., 2015
* OVOCs included in sensitivity tests of modeled OH and HO ₂ # Primary measurement.			

Detailed description of the OH Scavenging Inlet (OHSI)

The second and third paragraphs in Section 2.3 of the paper give an overview of the OH scavenging method used in ATom. Here we give additional detailed information on the design and operation of the OH Scavenging Inlet (OHSI).

Design

A cross-section of the OHSI shows that the ram-forced air enters the OHSI along its cylindrical axis, with the air flow coming from the right. The entrance is rounded to mimic the shape of a jet engine cowling. The total OHSI length is 7 cm. The OHSI is made of aluminum with an inner sleeve of Teflon. The C₃F₆/N₂ injection occurs 1 cm into the cylinder (1.25 cm dia.), which then slowly opens up to a larger cylinder (1.8 cm dia.). The distance between the injectors (0.02 cm inside dia.) and the sampling inlet is 3.0 cm. The truncated conical inlet OH detection flow tube sticks into the cylinder by 0.5 cm, enough to sample from the center of the airflow but not enough to substantially block the flow. The larger gray disk at the aft has 5 holes (6 mm dia.) and is used to slow the air flow in the OHSI. Prior to ATom, it took us 4 flights to adjust the hole sizes in the disk before sufficient OH scavenging was achieved.

Operation

The OH scavenging efficiency was measured by adding prodigious amounts of OH to the air just in front of the OHSI using two 185nm UV lamps embedded in the ATHOS inner nacelle and monitoring the OH signal with and without the addition of the C₃F₆ scavenger. The 70-sccm N₂ flow was kept on all the time so that the addition of the ~1 sccm C₃F₆ flow did not change the

flow characteristics in the OHSI. The lamps were occasionally turned on in flight at different altitudes for enough time to measure the OH with and without C₃F₆ addition. These data were then fit as a function of altitude. For the 0.9 sccm flow used in ATom-1, the external OH removal was 82 ± 5 %, while for the 1.3 sccm flow used in ATom-2, -3, and -4, the OH removal was 91 ± 5 %. From the measurements over a large range of altitudes, these conversion efficiencies are altitude independent over as much of the troposphere as could be measured.

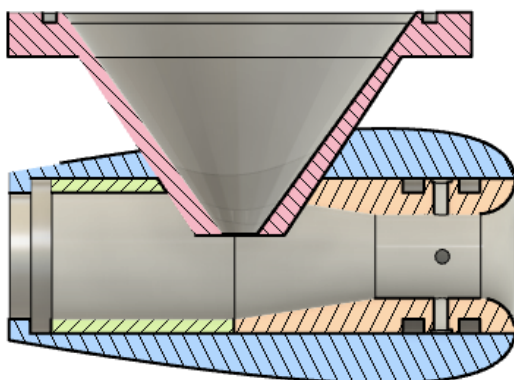


Figure S10. Cross sectional view of the OH Scavenging Inlet (OHSI). Air flows from right to left. The C₃F₆/N₂ mixture is injected through the small stainless- steel tubes denoted by gray rectangles and a gray circle 1 cm to the left of the OHSI entrance. The grey ring near the back is a disk with 5 holes (6 mm dia.) that slows the flow.

In the laboratory, the maximum internal OH removal as a function of C₃F₆ was measured by adding a 185nm UV lamp in the detection flow tube just underneath the inlet. This setup mimicked the production of possible interference OH just inside the inlet. Because interference OH is really more likely generated along the length of the detection flow tube, the laboratory values obtained for internal OH removal are likely overestimates. For the C₃F₆ flows used in ATom, the internal removal was less than 5%.

Direct measurement of the OH scavenging efficiency negates the need for understanding the flow characteristics in the OHSI. However, it is possible to determine the mean flow velocity inside the OHSI by using the measurements of the OHSI physical characteristics, the C₃F₆ flow rates, and the OH measurements with and without C₃F₆ addition, as in Equation S1.

$$v \text{ (cm s}^{-1}\text{)} = \sqrt{\frac{k_{OH+C_3F_6}(F_{C_3F_6}^2 - F_{C_3F_6}^1)2.69 \times 10^{19} x}{60 \ln(R_1/R_2) A}} \quad (\text{Eq. S1})$$

where $k_{OH+C_3F_6}$ is the OH+C₃F₆ reaction rate coefficient, $F_{C_3F_6}^i$ is the C₃F₆ flow rate (sccm), x is the distance between the injectors and the sampling inlet, R_i is the fraction of remaining OH signal for $F_{C_3F_6}^i$, and A is the OHSI internal cross-sectional area (cm²). The value 2.69×10^{19} is the number of molecules per cm³ for a standard atmosphere.

The resulting calculated velocity is 14 m s^{-1} . The resulting calculated reaction time is 0.0023 s . The Reynolds number varies from ~ 5000 at low altitudes to $\sim 10,000$ at high altitudes, suggesting turbulence is possible. However, the low variability in the OH signal suggests that the flow is not very turbulent. Using this velocity, we can check to see if the calculated and measured OH scavenging efficiencies agree. They do to within 5%. This agreement suggests that C_3F_6 is well-mixed within the OHSI and that the velocity gives self-consistent results. The resulting air flow rate is 90 LPM, well above the ~ 8 LPM that is drawn through the ATHOS inlet.

The rapid deceleration of the air as it decreases from aircraft speed of $\sim 200 \text{ m s}^{-1}$ to 15 m s^{-1} and the 90 LPM flow rate are quite hard to simulate in the laboratory. The calibration was done two ways. First air from the calibration wand flowed through the OHSI, perpendicular to the sampling inlet. Second, the OHSI was removed and the calibration wand was set so that the flow was almost directly into the sampling inlet, the method that has been used since 1996 (Faloona et al., 2004). The two methods gave similar calibration factors when the inlet size was large, but for smaller inlet sizes, the ratio of calibration factors of OHSI on to OHSI off became progressively smaller until it became unreasonably small at the smallest inlet sizes. The hypothesis is that OH was being lost on the smaller inlets. We decided that the calibration without the OHSI off gave more repeatable and realistic calibration factors.

Using the OHSI-less calibration method assumes that there is no OH loss on the OHSI or the ATHOS detection tube inlet. Two tests indicate that the OH wall loss on these surfaces is negligible. First, during the frequent aircraft pitch maneuvers for the MMS p, T, and winds measurement on the DC-8, the OH signal remained unchanged to within less than 10% as the aircraft pitch angle changed from $+4^\circ$ to -4° . If there was measurable loss on the inlet, it should have increased or decreased as the attack angle is changed by this much. Second, on two consecutive test flights for ATom 4, one was flown with the OHSI and one without. The two flights were in the same airmass and covered some of the same flight path at about the same time of day. Trace gases abundances were about the same to within 20%. The measured OH was the same to within 10% for the overlapping periods during the two flights. Thus, we have confidence that the calibration without the OHSI is accurate.

References.

- Adhikary, B., G. R. Carmichael, S. Kulkarni, C. Wei¹, Y. Tang, A. D’Allura¹, M. Mena-Carrasco, D. G. Streets, Q. Zhang, R. B. Pierce, J. A. Al-Saadi, L. K. Emmons, G. G. Pfister, M. A. Avery, J. D. Barrick, D. R. Blake, W. H. Brune, R. C. Cohen, J. E. Dibb, A. Fried, B. G. Heikes, L. G. Huey, D. W. O’Sullivan, G.W. Sachse, R. E. Shetter, H. B. Singh, T. L. Campos, C. A. Cantrell, F. M. Flocke, E. J. Dunlea, J. L. Jimenez, A. J. Weinheimer, J. D. Crouse, P. O. Wennberg, J. J. Schauer, E. A. Stone, D. A. Jaffe, and D. R. Reidmiller (2010). A regional scale modeling analysis of aerosol and trace gas distributions over the eastern Pacific during the INTEX-B field campaign, *Atmos. Chem. Phys.*, 10, 2091–2115. www.atmos-chem-phys.net/10/2091/2010/.
- Apel, E. C., R. S. Hornbrook, A. J. Hills, N. J. Blake, M. C. Barth, A. Weinheimer, C. Cantrell, S. A. Rutledge, B. Basarab, J. Crawford, G. Diskin, C. R. Homeyer, T. Campos, F. Flocke, A. Fried, D. R. Blake, W. Brune, I. Pollack, J. Peischl, T. Ryerson, P. O. Wennberg, J. D. Crouse, A. Wisthaler, T. Mikoviny, G. Huey, B. Heikes, D. O’Sullivan, and D. D. Riemer (2015). Upper tropospheric ozone production from lightning NO_x-impacted convection:

- Smoke ingestion case study from the DC3 campaign, *Journal of Geophysical Research: Atmospheres*, <https://doi.org/10.1002/2014JD022121>
- Brune, W.H., I.C. Faloona, D. Tan, A.J. Weinheimer, T. Campos, B.A. Ridley, S.A. Vay, J.E. Collins, G.W. Sachse, L. Jaegle and D.J. Jacobs (1998). Airborne in situ OH and HO₂ observations in cloud-free troposphere and lower stratosphere during SUCCESS. *Geophys. Res. Letters*, *25*, 1701-1704.
- Brune, W.H., X. Ren, L. Zhang, J. Mao, D.O. Miller, B. E. Anderson, D. R. Blake, R.C. Cohen, G. S. Diskin, S.R. Hall, T.F. Hanisco, L.G. Huey, B. A. Nault, J. Peischl, I. Pollack, T. B. Ryerson, T. Shingler, A. Sorooshian, K. Ullman, A. Wisthaler, and P.J. Wooldridge (2018). Atmospheric Oxidation in the Presence of Clouds during the Deep Convective Clouds and Chemistry (DC3) Study. *Atmos. Chem. Phys.*, *18*, 14493-14510. <https://doi.org/10.5194/acp-18-14493-2018>
- Cantrell, C.A., G.D. Edwards, S. Stephens, L. Mauldin, E. Kosciuch, and M. Zondlo (2003a). Peroxy radical observations using chemical ionization mass spectrometry during TOPSE. *J. Geophys. Res.*, *108*(D6), 8371. <https://doi:10.1029/2002JD002715>
- Cantrell, C.A., G.D. Edwards, S. Stephens, R.L. Mauldin, M.A. Zondlo, E. Kosciuch, F.L. Eisele, R.E. Shetter, B.L. Lefer, S. Hall, F. Flocke, A. Weinheimer, A. Fried, E. Apel, Y. Kondo, D.R. Blake, N.J. Blake, I.J. Simpson, A.R. Bandy, D.C. Thornton, B.G. Heikes, H.B. Singh, W.H. Brune, H. Harder, M. Martinez, D.J. Jacob, M.A. Avery, J.D. Barrick, G.W. Sachse, J.R. Olson, J.H. Crawford, and A.D. Clarke (2003b). Peroxy radical behavior during the Transport and Chemical Evolution over the Pacific (TRACE-P) campaign as measured aboard the NASA P-3B aircraft. *J. Geophys. Res.*, *108* (D20), art. no.-8797.
- Cantrell, C. A., L. Mauldin, M. Zondlo, F. Eisele, E. Kosciuch, R. Shetter, B. Lefer, S. Hall, T. Campos, B. Ridley, J. Walega, A. Fried, B. Wert, F. Flocke, A. Weinheimer, J. Hannigan, M. Coffey, E. Atlas, S. Stephens, B. Heikes, J. Snow, D. Blake, N. Blake, A. Katzenstein, J. Lopez, E. V. Browell, J. Dibb, E. Scheuer, G. Seid, and R. Talbot (2003c). Steady state free radical budgets and ozone photochemistry during TOPSE. *J. Geophys. Res.*, *108*(D4), 8361. <https://doi.org/10.1029/2002JD002198>
- Cazorla, M., G. M. Wolfe, S. A. Bailey, A. K. Swanson, H. L. Arkinson, and T. F. Hanisco, (2015). A new airborne laser-induced fluorescence instrument for in situ detection of formaldehyde throughout the troposphere and lower stratosphere. *Atmos. Meas. Tech.*, *8*, 541-552. <https://doi.org/10.5194/amt-8-541-2015>
- Chan, K. R., J. Dean-Day, S. W. Bowen, and T. P. Bui (1998). Turbulence measurements by the DC-8 meteorological measurement system. *Geophys. Res. Lett.*, *25*, 1355-1358. <https://doi.org/10.1029/97GL03590>
- Chen, G., D. Davis, J. Crawford, B. Heikes, D. O'Sullivan, M. Lee, F. Eisele, L. Mauldin, D. Tanner, J. Collins, J. Barrick, B. Anderson, D. Blake, J. Bradshaw, S. Sandholm, M. Carroll, G. Albercook, and A. Clarke (2001). An Assessment of the HO_x Chemistry in the Tropical Pacific Boundary Layer: Comparison of Model Simulations with Observations Recorded during PEM Tropics A. *J. Atmos. Chem.*, *38*, 317-344.
- Chen, H., A. Karion, C. W. Rella, J. Winderlich, C. Gerbig, A. Filges, P. P. Tans (2013). Accurate measurements of carbon monoxide in humid air using the cavity ring-down spectroscopy (CRDS) technique. *Atmos. Meas. Tech.*, *6*, 1031-1040. <https://doi.org/10.5194/amt-6-1031-2013>

- Colman, J. J., A. L. Swanson, S. Meinardi, B. C. Sive, D. R. Blake, and F. S. Rowland (2001). Description of the analysis of a wide range of volatile organic compounds in whole air samples collected during PEM-Tropics A and B. *Anal. Chem.*, *73*, 3723-3731. <https://doi.org/10.1021/ac010027g>
- Crouse, J. D., K. A. McKinney, A. J. Kwan, and P. O. Wennberg (2006). Measurement of gas-phase hydroperoxides by chemical ionization mass spectrometry. *Anal. Chem.*, *78*, 6726-6732. <https://doi.org/10.1021/ac0604235>
- Davis, D., G. Grodzinsk, G. Chen, J. Crawford, F. Eisele, L. Mauldin, D. Tanner, C. Cantrell, W. Brune, D. Tan, I. Faloona, B. Ridley, D. Montzka, J. Walega, F. Grahek, S. Sandholm, G. Sachse, S. Vay, B. Anderson, M. Avery, B. Heikes, J. Snow, D. O'Sullivan, R. Shetter, B. Lefer, D. Blake, N. Blake, M. Carroll, and Y. Wang (2001). Marine latitude/altitude OH distributions: Comparison of Pacific Ocean observations with models. *J. Geophys. Res.*, *106*, 32,691-32,707.
- Diskin, G. S., J. R. Podolske, G. W. Sachse, and T. A. Slate (2003). Open path airborne tunable diode laser hygrometer, 4817, 196, *International Society for Optics and Photonics*. <https://doi.org/225.10.1117/12.453736>
- Faloona, I., D. Tan, W. Brune, L. Jaeglé, D. Jacob, Y. Kondo, M. Koike, R. Chatfield, R. Pueschel, G. Ferry, G. Sachse, S. Vay, B. Anderson, J. Hannon, H. Fuelberg, (2000). Observations of HO_x and its relationship with NO_x in the upper troposphere during SONEX. *J. Geophys. Res.*, *105*, 3771-3783.
- Jaeglé, L., D.J. Jacob, W.H. Brune, D. Tan, I.C. Faloona, A.J. Weinheimer, B.A. Ridley, T.L. Campos, and G.W. Sachse (1998). Sources of HO_x and production of ozone in the upper troposphere over the United States. *Geophys. Res. Letters*, *25*, 1709-1712.
- Jaeglé, L., D. Jacob, W. Brune, I. Faloona, D. Tan, B. Heikes, Y. Kondo, G. Sachse, B. Anderson, G. Gregory, H. Singh, R. Pueschel, G. Ferry, D. Blake, and R. Shetter (2000). Photochemistry of HO_x in the upper troposphere at northern latitudes. *J. Geophys. Res.*, *105*, 3877-3892.
- Jaeglé, L., D.J. Jacob, W.H. Brune, and P.O. Wennberg (2001). Chemistry of HO_x radicals in the upper troposphere. *Atmos. Environ.*, *35*, 469-489.
- Mauldin III, R. L., D.J. Tanner, G.J. Frost, G. Chen, A.S.H. Prevot, D.D. Davis, and F.L. Eisele (1998). OH measurements during ACE-1: observations and model comparisons. *J. Geophys. Res. Atmos.*, *103*, 16713-16729.
- Mauldin III, R.L., D.J. Tanner, and F. L. Eisele (1999). Measurements of OH during PEM-Tropics A. *J. Geophys. Res.*, *104*, 5,817-5,827.
- Neuman, J. A., M. Trainer, S. S. Brown, K.-E. Min, J. B. Nowak, D. D. Parrish, and P. R. Veres (2016). HONO emission and production determined from airborne measurements over the Southeast US. *J. Geophys. Res. Atmos.*, *121*, 9237-9250. <https://doi.org/10.1002/2016JD025197>
- Olson, J.R., J. H. Crawford, G. Chen, A. Fried, M. J. Evans, C. E. Jordan, S. T. Sandholm, D. D. Davis, B. E. Anderson, M. A. Avery, J. D. Barrick, D. R. Blake, W. H. Brune, F. L. Eisele, F. Flocke, H. Harder, D. J. Jacob, Y. Kondo, B. L. Lefer, M. Martinez, R. L. Mauldin, G. W. Sachse, R. E. Shetter, H. B. Singh, R. W. Talbot, and D. Tan (2004). Testing fast photochemical theory during TRACE-P based on measurements of OH, HO₂, and CH₂O. *J. Geophys. Res.-Atmospheres*, *109*, Art. No. D15S10.

- Olson, J.R., J.H. Crawford, W. Brune, J. Mao, X. Ren, A. Fried, B. Anderson, E. Apel, M. Beaver, D. Blake, G. Chen, J. Crouse, J. Dibb, G. Diskin, S.R. Hall, L.G. Huey, D. Knapp, D. Richter, D. Riemer, J. St. Clair, K. Ullmann, J. Walega, P. Weibring, A. Weinheimer, P. Wennberg, and A. Wisthaler (2012). An analysis of fast photochemistry over high northern latitudes during spring and summer using in-situ observations from ARCTAS and TOPSE. *Atmos. Chem. Phys.*, *12*, 6799-6825. <https://doi.org/10.5194/acp-12-6799-2012>
- Regelin, E., H. Harder, M. Martinez, D. Kubistin, C. Tatum Ernest, H. Bozem, T. Klippel, Z. Hosaynali-Beygi, H. Fischer, R. Sander, P. Jöckel, R. Königstedt, and J. Lelieveld (2013). HO_x measurements in the summertime upper troposphere over Europe: a comparison of observations to a box model and a 3-D model. *Atmos. Chem. Phys.*, *13*, 10703-10720. <https://doi.org/10.5194/acp-13-10703-2013>
- Ren, X.R., J.R. Olson, J.H. Crawford, W.H. Brune, J.Q. Mao, R.B. Long, Z. Chen, G. Chen, M.A. Avery, G.W. Sachse, J.D. Barrick, G.S. Diskin, L.G. Huey, A. Fried, R.C. Cohen, B. Heikes, P.O. Wennberg, H.B. Singh, D.R. Blake, R.E. Shetter (2008). HO_x chemistry during INTEX-A 2004: Observation, model calculation, and comparison with previous studies. *J. Geophys. Res. Atmos.*, *113*, D5. doi: D05319.
- Ren, X., J. Mao, W.H. Brune, C.A. Cantrell, R.L. Mauldin, R.S. Hornbrook, E. Kosciuch, J.R. Olson, J.H. Crawford, G. Chen, H.B. Singh (2012). Airborne intercomparison of HO_x measurements using laser-induced fluorescence and chemical ionization mass spectrometry during ARCTAS. *Atmos. Meas. Tech.*, *5*, 2025-2037. <https://doi.org/10.5194/amt-5-2025-2012>
- Ryerson, T. B., E. J. Williams, and F. C. Fehsenfeld (2000). An efficient photolysis system for fast response NO₂ measurements. *J. Geophys. Res. Atmos.*, *105*, 26447-26461. <https://doi.org/10.1029/2000JD900389>
- Santoni, G. W., B. C. Daube, E. A. Kort, R. Jimenez, S. Park, J. V. Pittman, S. C. Wofsy (2014). Evaluation of the airborne quantum cascade laser spectrometer (QCLS) measurements of the carbon and greenhouse gas suite - CO₂, CH₄, N₂O, and CO - during the CalNex and HIPPO Campaigns. *Atmos. Meas. Tech.*, *7*, 1509-1526. <https://doi.org/10.5194/amt-7-1509-2014>
- Shetter, R. E. and M. Mueller (1999). Photolysis frequency measurements using actinic flux spectroradiometry during the PEM-Tropics mission: Instrumentation description and some results. *J. Geophys. Res. Atmos.*, *104*, 5647-5661. <https://doi.org/10.1029/98JD01381>
- Stone, D., M.J. Evans, R. Commane, T. Ingham, C.F.A. Floquet, J.B. McQuaid, D.M. Brookes, P.S. Monks, R. Purvis, J.F. Hamilton, J. Hopkins, J. Lee, A.C. Lewis, D. Stewart, J.G. Murphy, G. Mills, D. Oram, C.E. Reeves, and D.E. Heard (2010). HO_x observations over West Africa during AMMA: impact of isoprene and NO_x. *Atmos. Chem. Phys.*, *10*, 9415-9429. <https://doi.org/10.5194/acp-10-9415-2010>
- Stone, D., M. J. Evans, P. M. Edwards, R. Commane, T. Ingham, A. R. Rickard, D. M. Brookes, J. Hopkins, R. J. Leigh, A. C. Lewis, P. S. Monks, D. Oram, C. E. Reeves, D. Stewart, and D. E. Heard (2011). Isoprene oxidation mechanisms: measurements and modelling of OH and HO₂ over a South-East Asian tropical rainforest during the OP3 field campaign, *Atmos. Chem. Phys.*, *11*, 6749-6771, <https://doi.org/10.5194/acp-11-6749-2011>

- Stone, D.; M. J. Evans, H. M. Walker, T. Ingham, S. Vaughan, B. Ouyang, O. J. Kennedy, M. W. McLeod, R. L. Jones, J. Hopkins, S. Punjabi, R. Lidster, J. F. Hamilton, J. D. Lee, A. C. Lewis, L. J. Carpenter, G. Forster, D. E. Oram, C. E. Reeves, S. Bauguitte, W. Morgan, H. Coe, E. Aruffo, C. Dari-Salisburgo, F. Giammaria, P. Di Carlo, D. E. Heard (2014). Radical chemistry at night: comparisons between observed and modelled HO_x, NO₃ and N₂O₅ during the RONOCO project, *Atmos. Chem. Phys.*, **14**, 1299-1321
- Tan, D., I. Faloon, J. B. Simpas, W. Brune, J. Olson, J. Crawford, S. Sandholm, H.-W. Guan, T. Vaughn, J. Mastromarino, G. Sachse, S. Vay, J. Podolske, M. Avery, B. Heikes, J. Snow, H. Singh (2001). OH and HO₂ in the remote tropical Pacific: results from PEM-Tropics B. *J. Geophys. Res.*, **106**, 32,667.
- Wennberg, P.O., T.F. Hanisco, L. Jaegle, D.J. Jacob, E.J. Hints, E.J. Lanzendorf, J.G. Anderson, R.-S. Gao, E.R. Keim, S.G. Donnelly, L.A. Del Negro, D.W. Fahey, S.A. McKeen, R.J. Salawitch, C.R. Webster, R.D. May, R.L. Herman, M.H. Proffitt, J.J. Margitan, E.L. Atlas, S.M. Schauffler, F. Flocke, C.T. McElroy, and T.P. Bui (1998). Hydrogen radicals, nitrogen radicals, and the production of O₃ in the upper troposphere. *Science*, **279**, 49-53.